Retraction

Retracted: DenseNet-Based Classification of MRI Images for Detecting the Difference before and after Treating Liver Cancer

Scientific Programming

This article has been retracted by Hindawi following an investigation undertaken by the publisher [1]. This investigation has uncovered evidence of one or more of the following indicators of systematic manipulation of the publication process:

(1) Discrepancies in scope

(2) Discrepancies in the description of the research reported

(3) Discrepancies between the availability of data and the research described

(4) Inappropriate citations

(5) Incoherent, meaningless and/or irrelevant content included in the article

(6) Peer-review manipulation

The presence of these indicators undermines our confidence in the integrity of the article's content and we cannot, therefore, vouch for its reliability. Please note that this notice is intended solely to alert readers that the content of this article is unreliable. We have not investigated whether authors were aware of or involved in the systematic manipulation of the publication process.

In addition, our investigation has also shown that one or more of the following human-subject reporting requirements has not been met in this article: ethical approval by an Institutional Review Board (IRB) committee or equivalent, patient/participant consent to participate, and/or agreement to publish patient/participant details (where relevant).

Wiley and Hindawi regrets that the usual quality checks did not identify these issues before publication and have since put additional measures in place to safeguard research integrity.

We wish to credit our own Research Integrity and Research Publishing teams and anonymous and named external researchers and research integrity experts for contributing to this investigation.

The corresponding author, as the representative of all authors, has been given the opportunity to register their agreement or disagreement to this retraction. We have kept a record of any response received.

References

[1] J. Peng, "DenseNet-Based Classification of MRI Images for Detecting the Difference before and after Treating Liver Cancer," *Scientific Programming*, vol. 2021, Article ID 4609256, 8 pages, 2021.

Research Article

DenseNet-Based Classification of MRI Images for Detecting the Difference before and after Treating Liver Cancer

Jianbo Peng

Department of Radiology, Fengdu People's Hospital, 33 Lutang Street, Sanhe Street, Fengdu County, Chongqing 408200, China

Correspondence should be addressed to Jianbo Peng; 150511128@stu.sxit.edu.cn

This study aimed to explore the evaluation of Adriamycin-loaded microspheres in the treatment of liver cancer under DenseNet-based magnetic resonance imaging (MRI) image classification algorithm. According to different treatment methods, the research objects were classified into a normal saline (saline) group, a doxorubicin raw material (DOX) group, and a chitosan cross-linked pectin-doxorubicin conjugate macromolecular (CS-PDC-M) group. DenseNet's migration learning was employed to analyze the dynamic enhanced MRI characteristics and classify the MRI images. The CS-PDC-M-targeted nanotransfer system was examined with its apparent morphology, drug absorption, and cytotoxicity. Tumor volume was monitored using MRI, and alanine aminotransferase (ALT) and creatine kinase isoenzyme (CK-MB) values were detected. Results showed that the classification accuracy of liver cancer MRI image based on DenseNet model reached 80% at the arterial hepatobiliary stage. The DOX and CS-PDC-M group had obviously smaller tumor volume than that of the saline group ($P < 0.05$) with a statistical meaning. The mortality in the DOX group was 30%, while there was no death in the saline and CS-PDC-M groups. Compared with the saline and CS-PDC-M groups, ALT and CK-MB from the DOX group increased substantially ($P < 0.05$). Therefore, DOX had an inhibitory effect on tumor but damaged the heart and liver. DOX was used to construct CS-PDC-M that could maintain the original treatment effect of DOX and inhibit its side effects on the body, so CS-PDC-M had a clinical application value. In conclusion, Adriamycin-loaded microspheres could not only maintain the original therapeutic effect of Adriamycin but also inhibit its toxic and side effects on the body. The DenseNet model was applied in the liver cancer MRI dynamic image classification algorithm, and the normalization algorithm could improve the accuracy of the liver cancer microvessel classification, thus promoting the diagnostic efficiency of liver cancer diagnosis, which had clinical application value.

1. Introduction

Cancer is a disease that seriously harms human health in today's society, and there are 14 million new cancer patients (782,000 new liver cancer patients) and about 8.2 million deaths (745,000 deaths with liver cancer) worldwide each year [1]. Therefore, high mortality makes wary of scientists in the treatment of cancer research. Although surgical radical treatment is generally preferred in the early stage of cancer, there are no obvious symptoms in the early stage of cancer, and it cannot be detected in a timely manner. When a patient is diagnosed with cancer that is mostly at the middle and late stage, the cancer cells have spread or deteriorated, so that the patient cannot be cured by surgery. At present, interventional therapy is the main method of terminal-stage cancer treatment [2] and improves the tumor local drug concentration. What is more, it couples with slow-release and controlled-release effects to increase the drug effect time, so as to play the efficacy of chemotherapy drugs to an extreme. The local drug delivery can reduce the side and toxic effects of chemotherapy drugs in other tissues of the body, which provides a hope for patients with intermediate and terminal-stage cancer. The interventional therapy mainly includes renal artery chemoembolization, tumor microwave ablation, and cryoablation. In recent years, the cancer treatment research has become a hot topic due to the rise of molecular biology and the emergence of new theory, technology, and knowledge. Drug-loaded microsphere is a new embolism material, and microsphere technology has long-term slow-release or targeted effect

which can greatly improve the convenience and compliance of drug delivery for patients. Drug-loaded microsphere is a kind of potential dosage form which achieves the remarkable curative effect on the malignant tumor treatment of liver cancer [3]. DOX is one of the antitumor drugs with high anticancer activity and an effective broad spectrum and works on a variety of tumors, which belongs to the cycle nonspecific drug. It can destroy a variety of tumor cells that grow in the cycles [4–6]. Moreover, DOX (a drug for the treatment of liver cancer) is widely applied in clinical disease diagnosis [7, 8], but its side and toxic effects are also high on the normal tissues of the body. The main side and toxic effect is cardiac toxicity, and it can cause heart failure in severe cases. Then, the second is the damage to the medullary hematopoietic function, which reduces the number of platelets and white blood cells [9–11].

Medical imaging plays an important role in clinical disease diagnosis [12], and an imaging classification algorithm has good application value in the detection, nature, positioning, and staging of liver tumor cells [13]. The convolutional neural network (CNN) is a kind of feed-forward neural network with deep structure, which contains convolution computation. DenseNet, as a kind of CNN with the number of deeper layers, has high computational efficiency and storage efficiency, while greatly reducing the number of network parameters. Thus, the doctor combines the MRI images with clinical symptoms and serum biochemical indexes in the daily work, which can increase the accuracy of cancer diagnosis. Interventional treatment of liver cancer requires high imaging requirements [14–16] and also determines the formulation of treatment plans and the determination of treatment results. With the continuous development of science and technology, imaging technology is becoming more and more complex, and treatment plans and results are becoming more and more sophisticated and scientific.

The interventional treatment of liver cancer was the research object to prepare the chitosan cross-linked pectin-DOX nano-microspheres that were applied to the tumor cells of mice to investigate its curative effect and adverse reaction. The results of this study were designed to provide the theoretical basis for related research of DOX nano-microspheres in the clinical treatment of liver cancer.

2. Materials and Methods

2.1. Preparation of Doxorubicin-Loaded Chitosan Nanoparticles. About 0.05 g of pectin was added to 25 mL of distilled water and dissolved by heating. Then, 5 mg/mL sodium hydroxide was added to the aforementioned solution to adjust the pondus Hydrogenii (pH) to 5.0. The solution was stirred for 30 minutes and added with 0.06 g of N-Hydroxysuccinimide (NHS), and then, the mixed solution was stirred again for 30 minutes. About 0.025 g of DOX hydrochloride was weighed and added to 25 mL of distilled water to dissolve, so as to prepare a 5 mg/mL DOX hydrochloride solution. The solution was added to the pectin solution and stirred for 48 hours. After the reaction was completed, the solution was concentrated to 10 mL. The

concentrated solution was washed in anhydrous ethanol several times until the liquid supernatant was colorless. Then, the dark red solid was obtained and freeze-dried to get the pectin-DOX prodrug. Light should be avoided during the process.

The pectin-DOX prodrug was dissolved in the double-distilled water under the appropriate pH and temperature. Then, the dissolved solution was poured with 1 mg/mL chitosan solution at a constant speed, stirred for 8 hours, and loaded in to a dialysis bag. Besides, it was dialyzed in double-distilled water for 48 hours to get a CS-PDC-M solution. A 0.45 μm filter membrane was used to filter the residue to obtain a chitosan cross-linked pectin-DOX nano-microspheres.

2.2. Detection of Drug-Loading Capacity and Encapsulation Rate of Doxorubicin Nanoparticle-Loaded Chitosan. In Section 2.1, anhydrous ethanol included nonencapsulated DOX, which was obtained from washing the pectin-DOX prodrug. After repeated centrifugation, all the liquid supernatant was collected and blended. The ultraviolet (UV) absorption spectrophotometer was employed to detect the absorbance of liquid supernatant at the maximum absorption wavelength DOX, so as to calculate the content of free DOX. The dose of encapsulated DOX was the difference between total and free dose of DOX. The drug-loading capacity (LC%) was the ratio of the amount of encapsulated DOX to the mass of the carrier chitosan, and the encapsulation rate (EE%) was the ratio of the amount of encapsulated DOX to the total amount of DOX.

2.3. Characterization Analysis of Doxorubicin Nanoparticle-Loaded Chitosan. About 10 μL of CS-PDC-M solution was pipetted out onto a clean aluminum foil. Then, it was dried and sprayed with gold, and the morphology and size of the nanoparticles were observed under an electron microscope.

Dynamic diffusion method was applied to determine the drug release of CS-PDC-M in vitro. Specific experiments were as follows. Hydrochloric acid and Tris buffer salt were used to prepare buffer solutions with pH 7.4, 6.8, and 5.0. About 2 mL of CS-PDC-M solution was put into a dialysis bag, added to a 30 mL buffer solution, and vibrated in a thermostatic water bath at 37°C. Samples were taken at the 0th, 2th, 4th, 6th, 8th, 12th, 24th, 48th, 72th, 96th, 120th, 144th, 168th, 192th, 216th, and 240th hours. After sampling, the buffer was changed. The UV absorbance spectrophotometry was adopted to measure the absorbance to draw the standard curve diagram and calculate the cumulative concentration.

2.4. Cytotoxicity of Doxorubicin Nanoparticle-Loaded Chitosan. The human hepatocellular carcinoma HepG2 cell was used as the tumor cell model, and the toxicity of DOX preparation on human hepatocellular carcinoma HepG2 cells was evaluated by MTT assay. The cells in growth phase were collected and counted, and the cell suspension concentration was adjusted. The solution was inoculated on the

96-hole cell culture plate with $100 \mu L$ per hole, and the marginal holes were filled with sterile phosphate buffer saline (PBS). The culture plate was placed in an environment with 5% CO_2 at 37°C to cultivate for 24 hours. A 10% CS-PDC-M Dulbecco's modified Eagle's medium (DMEM) culture solution was prepared and taken in an Eppendorf (EP) tube with the amount of 3,600 mL. Then, $400 \mu L$ of CS-PDC-M solution with 19, 38, 76, 152, and $304 \mu g/mL$ was added into the EP tube. The tube was placed in an incubator at 30°C with 5% CO_2 and taken out at the 24th, 48th, and 72th hours. The culture solution was removed, $100 \mu L$ of $0.5 \mu g/mL$ MTT solution was added in the tube, and the tube was cultured again for 4 hours. Then, liquid supernatant was taken, and the absorbability of each hole was determined by enzyme-labeled instrument to calculate the relative survival rate.

2.5. Establishment and Imaging Examination of Liver Cancer Animal Model.

The mice bred in the animal Center of XXX University were selected in this study. Besides, they were aged about 6 to 7 weeks and weighed 28 to 33 g, with 12 males and 12 females, and fed with 0.5% ethyl methionine. They were administered drugs constantly for 8 to 9 months, so as to screen out the mice with symptoms of liver cancer as the experimental animal model. The selected mice were divided into three groups based on the different methods of liver cancer treatment, namely the saline group (mice were treated with normal saline), the DOX group (mice were given with DOX solution), and the CS-PDC-M group (mice were administered with DOX nano-microspheres). The experiment was started based on the experimental plan, the operation process was strictly regulated, and the ethical requirement was not violated.

GE3.0MR scanner and 8-channel head coil were applied to collect the magnetic resonance scanning parameters (fast-relaxation fast-spin echo (FRFSE) sequence, repetition time (TR) = 4600 ms, time of echo (TE) = 107 ms, layer thickness = 2.0 mm, field of view (FOV) = 24 cm × 18 cm, and matrix = 448 × 256). After image acquisition, signal intensity (SI) of T2-weighted imaging (T2WI) was calculated at different reagent doses of AFP-ultrasmall super-paramagnetic iron oxide (USPIO) and USPIO (150, 100, and 50), and signal-to-noise ratio (SNR) was calculated ($SNR = SI/SI_{background noise}$).

2.6. Construction of Image Classification Algorithm for Liver Cancer Based on DenseNet Model.

DenseNet was a convolution neural network with deep network levels, which was out of deepening the ResNet network layers and inception network structure to improve the fixed thinking pattern of network performance. There were the advantages of DenseNet as follows. It had less number of parameters compared with ResNet. The bypass strengthened the reuse of characteristics, so that the network was easier to train. What is more is that it had a reliable regularization effect to alleviate the gradient vanishing and model degradation. First, the input of the network was designed as a single channel based on the characteristics of the single channel of medical imaging. Second, with the advantage of DenseNet, the network theme adopted DenseBlock to construct the flowchart (Figure 1). Finally, a convolutional layer with the size of $1 \times 1 \times 1$ was added at the end of the network to reduce the number of full connections and further decrease the risk of network overfitting as shown in Figure 2. Finally, the data were processed as follows. The part of tumor data were for normalization operation, all the tumor data with large range difference were normalized to 0 to 1, and the equation was expressed as $\overline{x} = (X - min/max - min) \times 255$. In the aforementioned equation, X stood for any pixel value in the tumor of a mouse, min represented the minimum pixel value in the tumor pixel value, and max expressed the maximum pixel value in the tumor pixel value.

The process of image segmentation is as follows: (1) input liver cancer image; (2) preprocessing of liver cancer images, adjusting the image size to 126×126, and using RGB color processing method to adjust the image color; (3) the objects of this study were 18 hepatocellular carcinoma mouse models. A total of 23 hepatocellular carcinoma images were collected from each mouse, that is, 414 images, which were randomly divided into training sets (330 images) and verification sets (84 images) at a ratio of 4:1; (4) build the DenseNet model for image classification and train the model with the training set image; (5) use the validation set data to train the model validation; (6) the model gives the classification results and compares and analyzes the classification effect of the model.

The process of image segmentation was as follows. First, the liver cancer image was fed for processing. Second, the image was preprocessed to adjust the image size to 126×126, and the red-green-blue (RGB) color processing method was applied to adjust the image color. Third, the research objects of this study were 18 liver cancer mice models. Twenty-three liver cancer images were collected from each mouse, so the total was 414 images that were randomly divided into training sets (330 images) and validation sets (84 images) at a ratio of 4:1. Fourth, the DenseNet model was established for image classification, and the training set image was used for training the model. Fifth, the validation set image was adopted to validate whether the model was trained well. Sixth, the model produced the classification results, and the classification effect of the model was compared and analyzed.

2.7. In Vivo Experiments with Doxorubicin-Loaded Nanoparticles.

The selected tumors were all about 3.5 mm in diameter, and their volume was uniform. There were 18 well-grown mice (the ratio of male and female was 1:1) and divided evenly into three groups (the saline group, the DOX group, and the CS-PDC-M group). There were 6 mice in each group (3 male and 3 female mice). Besides, they received intravenous injection with the aforementioned preparation every 2 days (0.1 mL of the preparation was injected each time) and were weighed every 2 days. Their tumor size was measured, and mice were sacrificed at the 23th day to calculate the tumor volume.
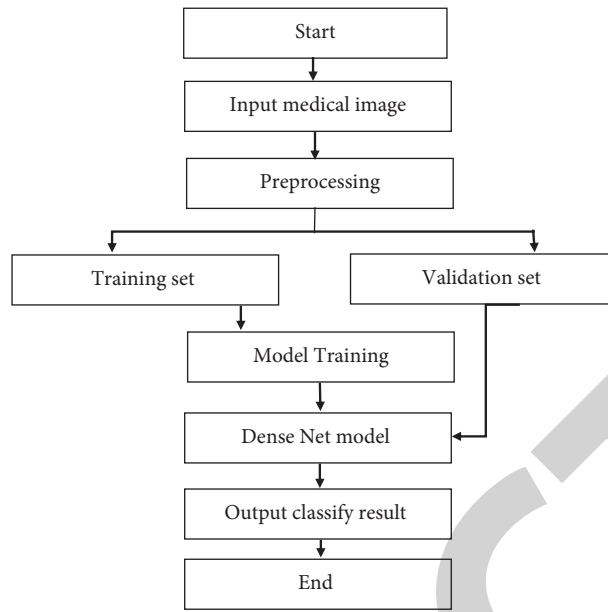
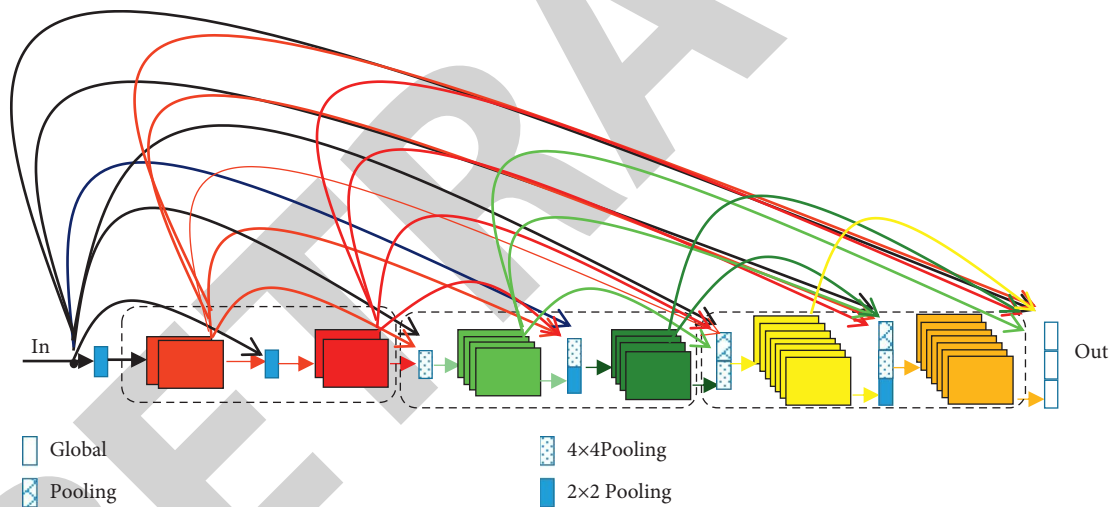FIGURE 1: Flowchart of imaging classification.

FIGURE 2: Basic structure of the DenseNet model.

2.8. Statistical Methods. SPSS version 19.0 statistical software was used to analyze the research data processing in this study, and the measurement data could be expressed as mean ± standard deviation ($\overline{x} \pm s$). In addition, count data were represented by percentage (%). The analysis of variance was used for pairwise comparison on the cell data of mice from the saline, DOX, and CS-PDC-M group. $P < 0.05$ meant that the results were statistically significant. Origin, version 7.5, was adopted to construct the graphs.

3. Results

3.1. Detection of CS-PDC-M. The surface characteristics of CS-PDC-M were observed by scanning electron microscope (SEM), as shown in Figure 3. The CS-PDC-M presented

irregular dispersion state with a diameter of about 200 nm, which met the quality standards of nano-microspheres.

3.2. Detection Results of the Drug-Loading Capacity and Encapsulation Rate of CS-PDC-M. The amount of free DOX was determined by UV, so as to calculate the drug-loading capacity and encapsulation rate of three batches of CS-PDC-M. The results of drug-loading capacity are shown in Tables 1 and 2, which indicated the results of encapsulation rate.

3.3. Drug Release Analysis of CS-PDC-M In Vitro. The in vitro drug release characteristics of CS-PDC-M were detected by dynamic diffusion method. Figure 4 shows the
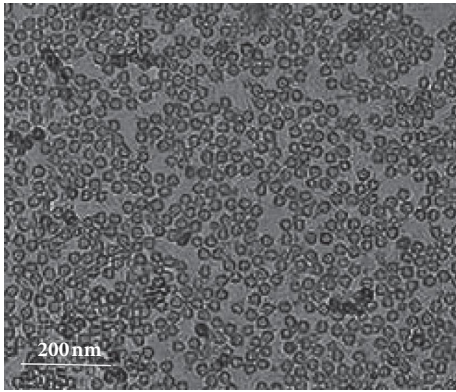
Figure 3: The SEM image of CS-PDC-M.

Table 1: Determination results of drug-loading capacity ($n = 3$).

Batch	Drug-loading capacity	RSD (%)
P_1	21.51 ± 1.33	
P_2	22.03 ± 1.13	3.11
P_3	23.05 ± 1.57	

Table 2: Determination results of encapsulation rate ($n = 3$).

Batch	Encapsulation rate	RSD (%)
P_1	53.43 ± 3.12	
P_2	55.15 ± 2.93	2.21
P_3	52.74 ± 3.04	

cumulative release curves of DOX nanotransfer system at different values of pH. The release rate of CS-PDC-M nanotransfer system was 68% at the 240th hour, and the CS-PDC-M nanotransfer system could realize the controllability of drug release to make blood drug concentration reach a stable level.

3.4. Cytotoxicity Experiment of CS-PDC-M In Vitro.
After the N1-S1 cells of all mice were processed, there were the flow cytometry detection results of cell necrosis rate in Figure 5. The fatality rate of mice in the DOX group was 2.86 times that of the saline group, reaching a remarkable level of difference ($P < 0.05$). In addition, the fatality rate of mice in the DOX group was 2.17 times that of the CS-PFC-M group, showing a statistically extreme difference ($P < 0.05$).

3.5. Analysis of Diagnostic Efficiency Based on DenseNet Liver Cancer MRI Image Classification Algorithm.
Figure 6 indicates the comparison between the MRI images of mouse liver cancer before and after the DenseNet model processing, and the images after processing had a high resolution. Table 3 reveals the accuracy of training set and validation set in detecting microvascular invasion of liver cancer at different periods. The classification accuracy of the constructed model was 80.05% and 76.51% in the training set and validation set at the hepatobiliary phase, respectively. Therefore, imaging classification algorithm had a good classification performance of the

hepatobiliary phase, and different network classification accuracy affects the classification effect of medical images. The imaging classification algorithm with higher accuracy could improve the screening efficiency, reduce the manpower cost, and decrease the misdiagnosis and missed diagnosis. Thus, the liver cancer imaging classification algorithm had good diagnostic efficiency in the diagnosis of liver cancer.

3.6. Antitumor Effects of CS-PDC-M.
Figure 7 indicates the change of mice tumor volume during the experiment and the survival rate of mice. At the 23rd day, the tumor volume of mice in the saline group was greater than that of CS-PDC-M group. It was proved that the CS-PDC-M had obvious inhibition for the tumor of mice. However, the tumor volume of mice in the DOX group was obviously smaller than that of the saline and CS-PDC-M, but several mice of the DOX group began to die at the 7th day. Moreover, they started to lose weight at the 10th day, which might be caused by the serious side and toxic effects of DOX. Thus, it could be concluded that the CS-PDC-M not only had inhibitory effect on tumor but also reduce its side and toxic effects.

3.7. Effects of CS-PDC-M on Damage of Organs.
Anthracycline-based drugs could often lead to cardiac toxicity. After the treatment effects were compared, clinical biochemical indexes of mice were collected, and the results are shown in Figure 8. There were increases on ALT and CK-MB of mice serum in the DOX group, indicating that DOX had damage to the heart and liver at the early phase. Some mice still died when reducing the dosage; thereby, it suggested that death was not caused by the size of the dose. Perhaps, the side and toxic effects of DOX resulted in death. However, the biochemical indexes of mice were normal in the CS-PDC-M group, showing that DOX nano-spheres could reduce the side and toxic effects of DOX on the body.

4. Discussion

MRI is a relatively new medical imaging technology and does not apply the harmful X-ray and hypersensitive contrast agents to the body. Furthermore, it can image in any direction, and various parameters of the imaging can provide more diagnostic information. MRI has high sensitivity and can fine contrast the differences between various tissues to achieve the advantages of multifunctional imaging and greatly promote the diagnostic efficiency of cancer. Therefore, MRI is one of the frequently used methods for the clinical detection of liver cancer. At present, a large number of studies have proved that MRI classification based on tumor imaging classification algorithm has a high accuracy rate in the treatment of liver cancer [17, 18].

DOX is an antitumor commonly applied drug in clinical disease diagnosis, which can affect the activity of topoisomerase II to play an antitumor role in the body. In addition, DOX has toxic effects on peripheral nerves and can damage the heart and liver. Nano preparation is a new type of pharmaceutical preparation that is developed by
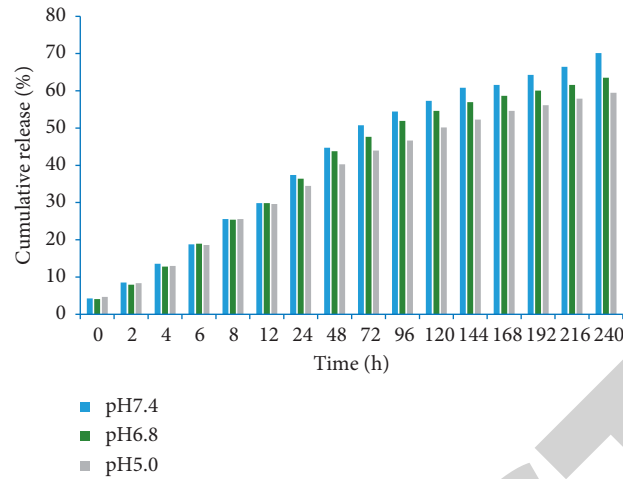
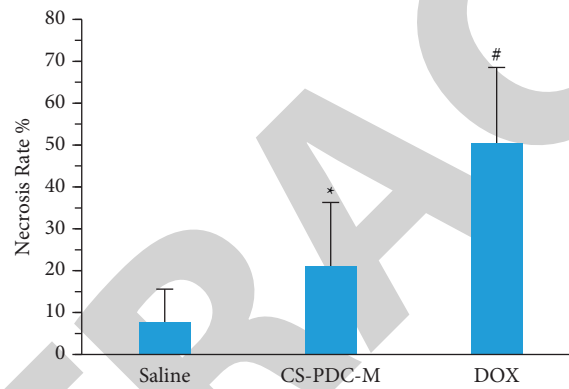Figure 4: In vitro release curves of CS-PDC-M under the environment with different values of pH.

Figure 5: Statistical chart of cell necrosis rate of mice in each group. Note: * indicated that the difference was statistically obvious compared with the saline group ($P < 0.05$); # expressed that there were statistically significant differences in contrast to the CS-PDC-M group ($P < 0.05$).
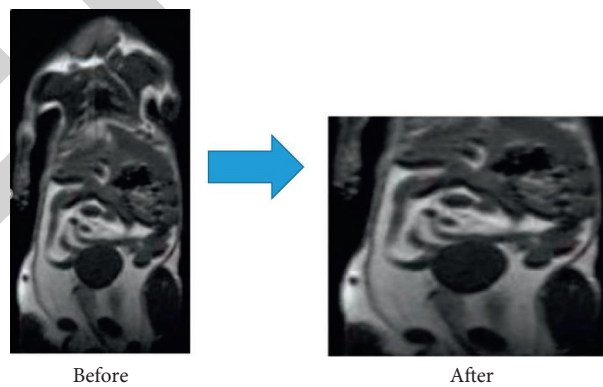

Figure 6: Comparison on the MRI images of mice before and after pretreatment.

Table 3: Classification accuracy of liver cancer images based on DenseNet model.

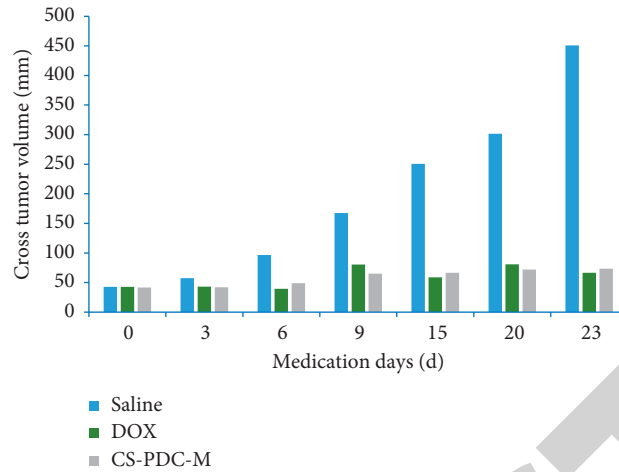| Stage	Training set		Validation set	
	CNN (%)	Our method (%)	CNN (%)	Our method (%)
Early arterial stage	65.92	75.98	55.87	62.46
Middle arterial stage	63.78	72.55	65.67	72.32
Late arterial stage	61.67	73.78	55.91	62.04
Hepatobiliary stage	71.23	80.05	68.45	76.51

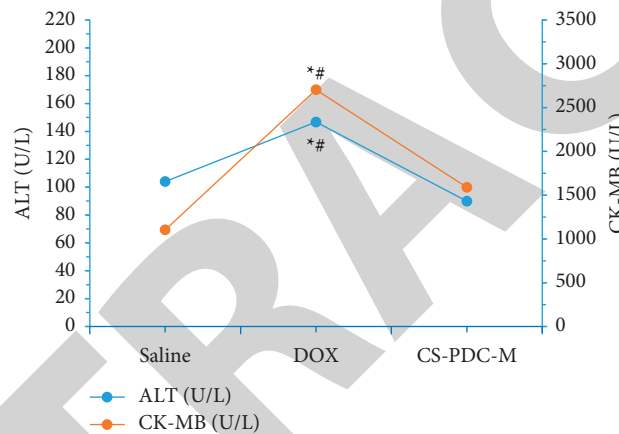Figure 7: Tumor volume changes of mice after administration.

Figure 8: Monitoring images of ALT and CK-MB in mice serum of the three groups. Note: * indicated that the difference was statistically substantial compared to the CS-PDC-M group ($P < 0.05$); # meant that there was a statistically great difference in contrast to the CS-PDC-M group ($P < 0.05$).

nanocarrier technology. By comparing with the traditional formulation, it can improve medication compliance, increase the local blood drug concentration, enhance drug curative effect, and effectively decrease side effects. CS-PDC-M was prepared in this study for the investigation of its in vitro cell toxicity and treatment effect of tumor volume in mice, the results showed that CS-PDC-M reduced the toxicity of DOX to the heart and liver during the treatment in contrast to the curative effect of traditional formulation. ALT mainly exists in the liver cells, and the liver cells are seriously damaged when ALT increases. CK-MB is an important marker for the diagnosis of acute myocardial infarction, and CK-MB is released into the blood when the myocardial tissue is damaged.

The tumor volume of mice in the CS-PDC-M group was smaller obviously than that of the saline group, suggesting that DOX had inhibitory effect on tumor cells. However, mice of the DOX group died earlier than the CS-PDC-M group. Some mice still died even when reducing the dosage. Thus, excessive doses of DOX were not suspected to be the cause of death, and its side and toxic effects led to the death.

What is more, the biochemical indexes of mice were compared again. It was found that ALT and CK-MB of mice in the DOX group were much higher than those of the other two groups. Elevation of ALT meant liver damage, and growth of CK-MB indicated there was impaired heart function of mice. Besides, the biochemical indexes of mice in the CS-PDC-M group tended to be normal, revealing that the CS-PDC-M nanotransfer system could reduce the side and toxic effects of DOX. It was consistent with the results of Wang et al. [19] and Wang et al. [20]. Therefore, CS-PDC-M had better application value in interventional therapy of liver cancer.

5. Conclusion

The liver cancer imaging classification algorithm could promote the accuracy of MRI in the diagnosis of liver cancer treatment. The application of CS-PDC-M in tumor cells of mice could effectively inhibit the growth of liver tumor, reduce the toxicity of DOX to other tissues, and avoid the heart and liver injury caused by DOX. The results could be a

reference but could not completely explain that the mechanism of CS-PDC-M in this study was completely consistent with that in the human body based on animal experiments and cytotoxic experiments. Therefore, it was necessary to further explore the therapeutic effect of CS-PDC-M in patients with liver cancer to investigate its effects of interventional therapy of liver cancer, so as to better play its clinical application value. This study provides a basis for future clinical studies on Adriamycin nanoparticles in the treatment of liver cancer.

Data Availability

The data used to support the findings of this study are available from the corresponding author upon request.

Conflicts of Interest

The authors declare no conflicts of interest.

References

[1] L. A. Torre, F. Bray, R. L. Siegel, J. Ferlay, J. Lortet-Tieulent, and A. Jemal, "Global cancer statistics, 2012," *CA: A Cancer Journal for Clinicians*, vol. 65, no. 2, pp. 87–108, 2015.

[2] J. Kettenbach, A. Stadler, I. v. Katzler et al., "Drug-loaded microspheres for the treatment of liver cancer: review of current results," *CardioVascular and Interventional Radiology*, vol. 31, no. 3, pp. 468–476, 2008.

[3] C. H. Wu, C. H. Lan, K. L. Wu et al., "Hepatocellular carcinoma-targeted nanoparticles for cancer therapy," *International Journal of Oncology*, vol. 52, no. 2, pp. 389–401, 2018.

[4] Y. Liu, L. Liu, Y. Zhou et al., "CKLF1 enhances inflammation-mediated carcinogenesis and prevents doxorubicin-induced apoptosis via IL6/STAT3 signaling in HCC," *Clinical Cancer Research*, vol. 25, no. 13, pp. 4141–4154, 2019.

[5] T. Yang, G. Du, Y. Cui et al., "pH-sensitive doxorubicin-loaded polymeric nanocomplex based on β-cyclodextrin for liver cancer-targeted therapy," *International Journal of Nanomedicine*, vol. 14, pp. 1997–2010, 2019.

[6] K. T. Brown, R. K. Do, M. Gonen et al., "Randomized trial of hepatic artery embolization for hepatocellular carcinoma using doxorubicin-eluting microspheres compared with embolization with microspheres alone," *Journal of Clinical Oncology*, vol. 34, no. 17, pp. 2046–2053, 2016.

[7] D. Chen, X. Pan, F. Xie et al., "Codelivery of doxorubicin and elacridar to target both liver cancer cells and stem cells by polylactide-co-glycolide/d-alpha-tocopherol polyethylene glycol 1000 succinate nanoparticles," *International Journal of Nanomedicine*, vol. 13, pp. 6855–6870, 2018.

[8] T. Yang, Y. Lan, M. Cao et al., "Glycyrrhetinic acid-conjugated polymeric prodrug micelles co-delivered with doxorubicin as combination therapy treatment for liver cancer," *Colloids and Surfaces B: Biointerfaces*, vol. 175, pp. 106–115, 2019.

[9] P. A. J. Speth, Q. G. C. M. Van Hoesel, and C. Haanen, "Clinical pharmacokinetics of doxorubicin," *Clinical Pharmacokinetics*, vol. 15, no. 1, pp. 15–31, 1988.

[10] K. Renu, V Abilash, and P Tirupathi, "Molecular mechanism of doxorubicin-induced cardiomyopathy-an update," *European Journal of Pharmacology*, vol. 818, pp. 241–253, 2018.

[11] C. Carvalho, R. X. Santos, S. Cardoso et al., "Doxorubicin: the good, the bad and the ugly effect," *Current Medicinal Chemistry*, vol. 16, no. 25, pp. 3267–3285, 2009.

[12] G. Litjens, T. Kooi, B. E. Bejnordi et al., "A survey on deep learning in medical image analysis," *Medical Image Analysis*, vol. 42, pp. 60–88, 2017.

[13] E. Sagrini, M. Iavarone, F. Stefanini et al., "Imaging of combined hepatocellular-cholangiocarcinoma in cirrhosis and risk of false diagnosis of hepatocellular carcinoma," *United European Gastroenterology Journal*, vol. 7, no. 1, pp. 69–77, 2019.

[14] L. M. Wang, H. J. Qiao, W. Sun, and Z. Li, "Research on correlations of magnetic resonance imaging features and pathological changes in liver cancer with Beclin1 expression," *European Review for Medical and Pharmacological Sciences*, vol. 23, no. 6, pp. 2409–2416, 2019.

[15] S. Li, S. Shi, A. Li, H. Liu, and L. Cai, "Diffusion-weighted magnetic resonance imaging in assessment of primary liver cancer after HIFU treatment," *Journal of College of Physicians and Surgeons Pakistan*, vol. 29, no. 4, pp. 305–308, 2019.

[16] R. Xu, J. Wang, X. Huang et al., "Clinical value of spectral CT imaging combined with AFP in identifying liver cancer and hepatic focal nodular hyperplasia," *Journal of Buon*, vol. 24, no. 4, pp. 1429–1434, 2019.

[17] T. H. Kim, S. Y. Kim, A. Tang, and J. Lee, "Comparison of international guidelines for noninvasive diagnosis of hepatocellular carcinoma: 2018 update," *Clinical and Molecular Hepatology*, vol. 25, no. 3, pp. 245–263, 2019.

[18] A. Carrillo, J. L. Duerk, J. S. Lewin, and D. Wilson, "Semi-automatic 3-D image registration as applied to interventional MRI liver cancer treatment," *IEEE Transactions on Medical Imaging*, vol. 19, no. 3, pp. 175–185, 2000.

[19] Q. Wang, L. Gao, X. Zhu et al., "Co-delivery of glycyrrhizin and doxorubicin by alginate nanogel particles attenuates the activation of macrophage and enhances the therapeutic efficacy for hepatocellular carcinoma," *Theranostics*, vol. 9, no. 21, pp. 6239–6255, 2019.

[20] H. Wang, M. Zheng, J. Gao et al., "Uptake and release profiles of PEGylated liposomal doxorubicin nanoparticles: a comprehensive picture based on separate determination of encapsulated and total drug concentrations in tissues of tumor-bearing mice," *Talanta*, vol. 208, Article ID 120358, 2020.